Geophysical Research Letters

RESEARCH LETTER
10.1029/2024GL110176

Improved Temperature-Dependent Ice Refractive Index Compilation in the Far-Infrared Spectrum

Siheng Wang[1], Tong Ren[1], Ping Yang[1], Masanori Saito[2], and Helen E. Brindley[3]

[1]Department of Atmospheric Sciences, Texas A&M University, College Station, TX, USA, [2]Department of Atmospheric Science, University of Wyoming, Laramie, WY, USA, [3]Department of Physics, National Centre for Earth Observation, Imperial College London, Kensington, UK

Key Points:

- A new compilation of ice refractive index covering the entire solar and terrestrial thermal spectrum is presented
- This study focuses on the far-infrared spectrum, which is not well studied but accounts for most terrestrial emissions in cold regions
- Implications of improved ice cloud modeling with temperature-dependent ice refractive indices are discussed

Supporting Information:

Supporting Information may be found in the online version of this article.

Correspondence to:

P. Yang,
pyang@tamu.edu

Citation:

Wang, S., Ren, T., Yang, P., Saito, M., & Brindley, H. E. (2024). Improved temperature-dependent ice refractive index compilation in the far-infrared spectrum. *Geophysical Research Letters*, *51*, e2024GL110176. https://doi.org/10.1029/2024GL110176

Received 8 MAY 2024
Accepted 24 JUN 2024

Author Contributions:

Conceptualization: Siheng Wang, Ping Yang
Formal analysis: Siheng Wang, Tong Ren
Funding acquisition: Siheng Wang, Ping Yang, Masanori Saito
Project administration: Siheng Wang, Ping Yang
Software: Siheng Wang, Tong Ren
Supervision: Siheng Wang, Ping Yang
Visualization: Siheng Wang, Tong Ren
Writing – original draft: Siheng Wang, Tong Ren
Writing – review & editing: Siheng Wang, Ping Yang, Masanori Saito, Helen E. Brindley

Abstract A new ice refractive index compilation is reported for a broad spectrum ranging from 0.0443 to 10^6 μm, focusing on the pronounced temperature-dependence of ice optical properties in the far-infrared (far-IR) segment (15–100 μm). A sensitivity study assuming spherical particles shows that selecting ice refractive indices at 12 temperatures and 215 wavelengths in the far-IR region gives sufficient accuracy in interpolated refractive indices for developing a new ice crystal optical property database. Furthermore, we demonstrate the differences between the bulk single-scattering properties computed for hexagonal ice particles with this new compilation compared to a previous iteration at three far-IR wavelengths where substantial differences are noticed between the two ice refractive index compilations. We suggest that our new ice refractive index data set will improve downstream light-scattering applications for upcoming far-IR satellite missions and allow robust modeling of outgoing longwave radiation under ice cloud conditions.

Plain Language Summary An imbalance between absorbed solar energy at ultraviolet (0.01–0.38 μm), visible (0.38–0.75 μm), and near-infrared (IR) (0.75–2.5 μm) wavelengths and outgoing longwave radiation energy emitted from the Earth at mid-IR (2.5–15 μm) and far-IR (15–100 μm) wavelengths leads the surface temperature to change. Solar and mid-IR energy is well-observed by satellite sensors. However, it has been challenging to conduct spaceborne radiometric measurements in the far-IR regime, which accounts for more than half of the OLR in cold areas such as polar regions. This study develops a new compilation of temperature-dependent ice refractive index for application to the first far-IR satellite missions extending beyond 25 microns, particularly toward a better understanding of ice clouds. It is shown that the improvements in the ice refractive index have a substantial impact on downstream light-scattering computation in the far-IR regime. Furthermore, the present study also explores adequate spectral and temperature resolutions for computing a new ice cloud optical property database to guarantee that the optical property values at other wavelengths and temperatures not included in the direct light-scattering computations can be accurately obtained through interpolation.

1. Introduction

Almost all Earth-atmosphere outgoing longwave (LW) radiation (outgoing longwave radiation (OLR)) is in the infrared (IR) spectral region from wavelengths (λ) 2.5–100 μm, with, in the global mean, roughly half in the well-measured mid-IR region (2.5–15 μm) and half in the far-IR region (15–100 μm) (Harries et al., 2008). While the distinction between far-IR and microwaves is not absolute, the present far-IR region refers to the spectral segment from 15 to 100 μm to match with the upper wavelength cutoff of the upcoming far-IR instruments. Historically, the far-IR spectrum has been poorly measured due to difficulties in developing sensors capable of capturing the low energy photons in this spectral regime with sufficient accuracy.

However, growing interest in the potential utility of spectral variations of far-IR OLR for understanding climate model deficiencies and modulating climate feedback (e.g., Chen et al., 2014; Huang et al., 2008; Huang et al., 2010; Roemer et al., 2023; Wei et al., 2023; Zender & Kiehl, 1997), coupled with advances in compact, uncooled far-IR detectors and rapid computational processing, have motivated the development of new far-IR satellite missions, including the Polar Radiant Energy in the Far Infrared Experiment (PREFIRE) (L'Ecuyer et al., 2021) and the Far-infrared-Outgoing-Radiation Understanding and Monitoring (FORUM) (Palchetti et al., 2020).

Far-IR observations are highly sensitive to ice clouds. Early theoretical studies implied that measurements of the outgoing far-IR spectrum should give unique information of crystal habit and size distribution (Yang et al., 2003).

More recent work has demonstrated that measurements of ice cloud optical properties across the full IR range can improve the quantification of cloud optical thicknesses and effective sizes of ice clouds under nighttime conditions robustly when visible and near-IR solar-band measurements are unavailable (Saito et al., 2020). Nonetheless, work exploiting airborne observations of far-IR radiances in the presence of cirrus clouds demonstrate an inability to simulate measurements consistently across the far-IR and Mid-IR spectrum using available ice-cloud bulk optical property data sets (Bantges et al., 2020; Cox et al., 2010). This is a serious issue, especially given recent modeling work highlighting the marked impact of longwave scattering in the presence of ice cloud on atmospheric heating rates (e.g., Fan et al., 2023; Kuo et al., 2017; Ren et al., 2020), motivating the development of an improved database of ice cloud optical properties.

Developing an ice cloud optical property database requires knowledges of not only ice particle shapes/habits (Lawson et al., 2019), but also the real (n) and imaginary (k) parts of the ice refractive index in the spectral range of interest. The quantity k is a measure of ice absorbance, and it is easier to measure k than quantity n (Warren, 1984). Consequently, an ice refractive index compilation over the entire solar and terrestrial thermal spectral range firstly calculates k based on measurements and analytic formulae empirically fitted to measurements. The quantity k varies by 10 orders of magnitude across the wavelength and temperature ranges. The compilation is subsequently followed by calculating n that is of the order unity at all wavelengths, using the Kramers-Kronig (K-K) relation (Jackson, 1999; Warren, 1984). Current ice cloud optical property models have been developed for Earth observing sensors measuring at visible to mid-IR wavelengths and integrating across the broadband reflected shortwave and outgoing longwave spectrum (e.g., Loeb et al., 2018; Yang et al., 2013). However, they do not consider the temperature-dependence of ice refractive indices, which becomes pronounced as λ increases to the far-IR region (Iwabuchi & Yang, 2011) because lattice vibrations important to ice far-IR radiation absorption shift to longer λ as temperature increases (Warren, 2019).

Ice refractive indices compiled by Warren and Brandt (2008) (hereinafter referred to as WB08), covering the entire solar and terrestrial radiative range from 0.0443 to 10^6 μm at constant temperature $T = 266$ K, have been extensively used in modeling ice particle optical properties involved in Earth, planetary, and astrophysical research (e.g., Dang et al., 2016; Khuller et al., 2021). It is also worth mentioning that Jiang and Wu (2004) developed a temperature-dependent ice refractive index model at near-millimeter and sub-millimeter wavelengths. Using the compilation involved in WB08 and six other data sets (Table S1 in Supporting Information S1), Iwabuchi and Yang (2011) (hereinafter referred to as IY11) developed a temperature-dependent data set of ice refractive index, which also spans 0.0443–10^6 μm at 12 temperatures from 160 to 270 K in 10 K increments. This data set has been used to model frozen hydrometeor optical properties in the microwave (MW) region (Ding et al., 2017; Ren et al., 2023), where the temperature-dependence of ice optical constants is most significant. However, IY11 indicated that more reliable measurements were needed in the spectral region between 70 and 300 μm. Besides the data of WB08, the only measurement-based k data in the far-IR region included in IY11 are those of Curtis et al. (2005) (hereinafter referred to as Cu05). The WB08 k values at 266 K in the 26–200 μm region were obtained by extrapolating the k values of Cu05 at the 3 highest of the 8 total measurement temperatures (156, 166, and 176 K) to 266 K via fitted analytical functions (Warren & Brandt, 2008).

Based on transmittance measurements of ice films formed via direct water vapor deposition and a more accurate method to determine the thicknesses of ice films than previous studies, Cu05 calculated ice optical constants between 106 and 176 K from 15 to 200 μm. The k data of Cu05 are noisy at $\lambda > 80$ μm, and hence IY11 chose to smooth the k data using the k value of Cu05 at 75 μm and the k formula of Mätzler (2006) for each selected λ between 75 and 192 μm. In a more recent study, astrophysicists measured ice layer transmittances at 6 temperatures between 10 and 250 K over the spectral range between 80 and 625 μm (Reinert et al., 2015, hereafter Re15). By fitting coefficients to the measurements, Re15 proposed empirical formulae to calculate k between 10 and 250 K in the spectral range starting from 94 μm to longer λ depending upon temperature. Because of the uncertainties in the k values of IY11 from 70 to 300 μm, the availability of more recently developed temperature-dependent k computational formulae from Re15 and the identified issue in simulating ice-cloud observations across the far-IR, in this paper our goal is to improve the ice refractive index over the entire range of wavelengths and temperatures relevant to atmospheric research.

Given the ice refractive index data at wavelengths, temperatures of interest, and an assumed ice particle habit, ice particle single-scattering properties can be computed (Yang et al., 2019). An ice particle single-scattering property database is basically an archive of computed properties for a large set of input parameters,

particularly wavelengths, temperatures, particle sizes, and particle habits. To minimize the computational effort of developing a new temperature-dependent far-IR ice cloud optical property database, in this study we explore an appropriate selection of the temperatures and wavelengths for single-scattering computation to ensure that the optical property values at off-database-grid-point temperatures and wavelengths can be accurately obtained via interpolation.

2. Methods

Existing ice optical property data sets are often based on the WB08 ice refractive index compilation and computed at a low resolution in the far-IR region. IY11 computed ice refractive indices at 2,000 logarithmically spaced wavelengths between 0.0443 and 2×10^6 μm, resulting in 215 wavelengths in the 15–100 μm range, and at 12 temperatures from 160 to 270 K with an increment of 10 K. However, some IY11 refractive index values were estimated based on incomplete measurements due to a lack of data availability, as discussed above.

The present new ice refractive index compilation adopts all the 12 temperatures and 2,000 wavelengths selected in IY11. The k values are first obtained via linear interpolations and extrapolations in log λ and T based on the databases in Table S1 in Supporting Information S1, and the K-K relation is subsequently applied to compute n values with the k values. We incorporate the new Re15 empirical formulae to compute k values in the 94–451 μm λ range and the k formulae of Mätzler (2006) from $\lambda = 750$ to 10^6 μm; the k values are interpolated linearly to wavelengths between 451 and 750 μm to guarantee a smooth transition in this λ region. As in IY11, two anchor points at 0.632 and 10^6 μm are used to iteratively adjust k values in the X-ray and far-IR regions until computed n values at the two anchor points converge to their known values.

While new ice refractive index compilation accounts for temperature-dependence, it requires further effort to establish an ice cloud optical property data set for application to observations from a specific spaceborne far-IR instrument. For example, the FORUM Sounding Instrument is expected to have at least 0.5 cm^{-1} nominal resolution in the far-IR region from wavenumbers 1,600 to 100 cm^{-1} (or ≈3,000 wavelengths from 6.25 to 99.50 μm, a higher resolution than in IY11) (Palchetti et al., 2020), resulting in λ resolutions of ≈0.002 μm at the 6.25 μm lower bound and ≈0.49 μm at the 99.50 μm upper bound. If an ice particle single-scattering property database with a lower spectral resolution is developed to facilitate FORUM applications, errors may be introduced in single-scattering properties interpolated to wavelengths and temperatures not included in the database. It is hence necessary to quantify the interpolation errors. To this end, we estimate potential interpolation errors by computing the single-scattering properties assuming spherical ice particles in the present sensitivity study. This approach is taken to minimize computational effort because light-scattering computations involving nonspherical particles are extremely computationally intensive. While spherical particles are rare in ice clouds, their properties can be rapidly calculated using the efficient Lorenz-Mie code (Bohren & Huffman, 2008). Our final data set will be computed for various nonspherical habits, but relative errors in spectral and temperature interpolations for spherical and nonspherical particles are expected to be similar because the ice refractive index is determined by the wavelength and temperature but independent of ice particle habit. Based on this hypothesis, the interpolation errors quantified in the case of ice spheres provides valuable guidance to specifying the spectral and temperature resolutions for developing a practical database of the single-scattering properties of nonspherical ice crystals.

Of the 2,000 wavelengths in our new ice refractive index compilation, 215 wavelengths are in the far-IR between 15 and 100 μm. A user can derive the optical properties at any wavelength by interpolating between the values at the 215 wavelength grid points of the database. Here the maximum potential far-IR interpolation errors are estimated by adding 214 wavelengths logarithmically across the original 215 wavelengths, a total of 429 wavelengths. Similarly, another 11 temperatures distributed linearly across the original 12 temperatures are added to estimate interpolation errors in the temperature dimension. Refractive indices at the 429 wavelengths and the 23 temperatures are first regenerated based on the K-K relation. As stated above, we prepare the interpolation test based on the efficient Lorenz-Mie (Bohren & Huffman, 2008) computation of a spherical ice particle single-scattering property database at the 429 wavelengths and the 23 temperatures. This database is used as the benchmark to estimate interpolation errors. The Lorenz-Mie computations are performed for 3 spherical ice particle optical properties, namely, the extinction efficiency (Q_{ext}), single-scattering albedo (ω'), and asymmetry factor (g'). The 189 spherical ice radii used in this study match the effective radii (Foot, 1988; Saito & Yang, 2022) of the particle sizes in Coy et al. (2023).

The interpolation test selects computed spherical ice optical properties at the original 215 wavelengths and the 12 temperatures as the known values for subsequent interpolations. For the 189 stated particle sizes (this test does not interpolate across size), we interpolate linearly in log λ to the inserted 214 mid-point wavelengths and linearly to the 11 added temperatures (165, 175, 185, 195, 205, 215, 225, 235, 245, 255, 265 K) for comparison to those directly computed with refractive indices regenerated using the K-K relation (i.e., the benchmark values). To quantify the interpolation error for each optical property at each interpolated data point, the interpolation error is the interpolated value minus the benchmark value.

A second sensitivity study is performed to estimate the impact on the optical properties as a result of using our new refractive indices compared to those reported in IY11. As a common atmospheric ice particle shape, the hexagonal column has been extensively used in ice cloud optical property models (e.g., Fu, 1996; Fu et al., 1998), so we consider randomly oriented hexagonal columns with a fixed aspect ratio of 1 in the present computations. These computationally expensive nonspherical ice scattering computations are only performed at a few selected wavelengths and temperatures. A recent study shows that the majority of airborne in situ measured ice particles smaller than 50 μm have some degree of irregularity (Järvinen, Wernli, & Schnaiter, 2018). In ice cloud optical property models, the impact of this crystal complexity on optical properties may be simulated by particle surface roughness (Yang et al., 2013). Järvinen, Jourdan, et al. (2018) showed that featureless scattering phase functions produced in surface-roughened ice particle models agree with angular scattering measurements of in situ airborne polar nephelometers (e.g., Abdelmonem et al., 2016; Schnaiter et al., 2018). Therefore, the hexagonal columns are assumed to have severely roughened surfaces in our scattering computations.

In addition, bullet rosette ice crystals are frequently present within in situ-formed cirrus clouds (Lawson et al., 2019). We also perform light-scattering computations for the solid bullet rosette ice particles included in Yang et al. (2013) with our new refractive indices to demonstrate the sensitivity of computed ice cloud optical properties to ice particle shape. The bullet rosette ice particles are assumed to be randomly oriented and have severely roughened surfaces in the computations.

We use the improved geometric optics method (IGOM; Yang & Liou, 1996) to calculate single-scattering properties of hexagonal column and bullet rosette ice particles for 189 sizes (or maximum dimensions, $D_{\max}$) whose values are the same as those in Coy et al. (2023). The height of a hexagonal column is taken as its $D_{\max}$; the diameter of the circumscribed sphere of a bullet rosette particle is taken as its $D_{\max}$. Outside the geometric optics regime, IGOM is not accurate. Hence, for small ice particles ($(2\pi D_{\max})/\lambda < 50$), we use the Invariant Imbedding T-matrix method (IITM) (Bi & Yang, 2014; Zhang et al., 2022) for light-scattering computations. When a particle is small, the influence of surface roughness on single-scattering properties is small (Saito & Yang, 2022). After ice particle single-scattering property computations are completed with both IY11 and the present compilation, we calculate ice cloud bulk optical properties, namely the bulk mass extinction coefficient ($\beta_{\text{ext,m}}$), single-scattering albedo (ω), and asymmetry factor (g), using the cloud ice particle size distribution in the Thompson microphysics scheme (Thompson et al., 2004, 2008). The selection of the particle size distribution from a microphysics scheme in calculating ice cloud bulk optical properties results in a more consistent representation of ice cloud mass and mean particle size in model microphysics and radiation schemes, making radiation simulations more representative of the model simulated cloud conditions (Baran, 2012; Baran et al., 2014; Ren et al., 2021; Thompson et al., 2016).

The Thompson scheme assumes a gamma size distribution $N(D_{\max})$ for cloud ice:

$$N(D_{\max}) = N_0 D_{\max}^{\mu} e^{-\Lambda D_{\max}}, \tag{1}$$

where N_0, $\mu = 0$, and Λ are the intercept, shape, and slope parameters, respectively. As shown in previous studies (Saito & Yang, 2022; Wyser & Yang, 1998), it is advantageous to parameterize bulk optical properties as a function of the effective radius (r_{eff}), defined as follows:

$$r_{\text{eff}} = \frac{3\int_{D_{\max,l}}^{D_{\max,u}} V(D_{\max}) N(D_{\max}) \, dD_{\max}}{4\int_{D_{\max,l}}^{D_{\max,u}} A(D_{\max}) N(D_{\max}) \, dD_{\max}}, \tag{2}$$

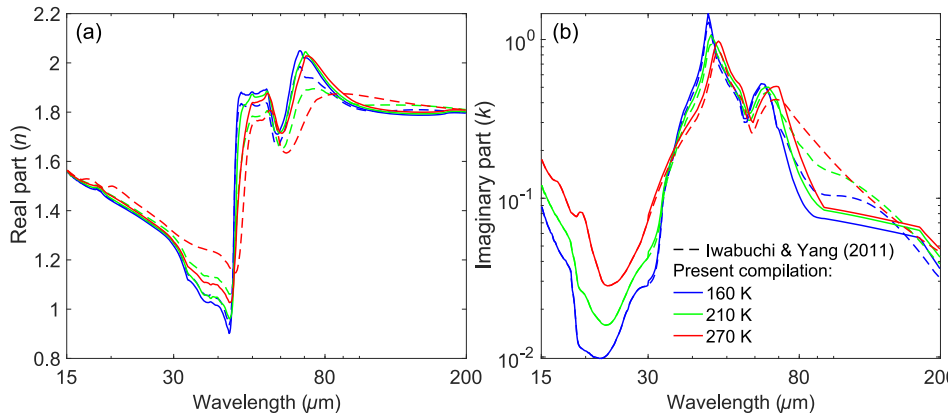

Figure 1. A comparison of (a) n and (b) k values in IY11 and the present compilation in the far-IR region at 3 different temperatures 160, 210, and 270 K. Solid lines are this work, dashed lines are from IY11. The x-axis extends to 200 μm to demonstrate that the changes beyond 100 μm are relatively small.

where $V(D_{max})$ and $A(D_{max})$ are ice volume and mean projected area, respectively; $D_{max,l}$ and $D_{max,u}$ are the lower and upper cutoffs of the maximum dimension. In addition, cloud ice particle size distributions assumed in a cloud microphysics scheme and a spaceborne remote sensing algorithm for inferring cloud properties are often different, although satellite-based cloud property retrievals are extensively used to evaluate climate models. We also calculate ice cloud bulk optical properties with the present ice refractive index compilation using the gamma size distribution with an effective variance of 0.1 adopted in the Moderate Resolution Imaging Spectroradiometer (MODIS) Collection 6 (MC6) cloud retrieval algorithm (Platnick et al., 2017). The differences in the ice cloud bulk optical properties calculated with the above two different particle size distributions are demonstrated in the present study.

3. Results

As described above, the main difference between the ice refractive index compilation described here and that of IY11 is that this study includes the more recent k formulae of Re15 in the far-IR region. Therefore, the n and k values show the most significant differences between compilations in the far-IR region (Figure 1). In Figure 1a, the largest difference in n appears to be around 70 μm, and in Figure 1b the most considerable differences in k appear to be around 45 and 90 μm. As temperature increases from 160 to 270 K, Figure 1a, in agreement with IY11, shows that n increases between about 15 and 45 μm and the two n peaks between 55 and 60 μm and between 65 and 90 μm shift to longer wavelengths. In Figure 1b, k increases with temperature between 15 and 35 μm and the two k peaks from ≈45 to 50 μm and from ≈60 to 75 μm also shift to longer wavelengths. The difference between n and k values from the two compilations also appears to increase with increasing temperature.

The first sensitivity study described in Section 2 tested interpolation errors for spherical ice particles using the new far-IR refractive index compilation shown in Figure 1 in the 15–100 μm range. The interpolations result in 1,377,243 (=189 × 215 × 11 + 189 × 214 × 23) values of each of the single-scattering properties, that is, Q_{ext}, ω′, and g'. Figure S1 in Supporting Information S1 shows the benchmark and the differences between interpolated and benchmark Q_{ext}, ω′, and g' of the spherical ice with a radius of 30.45 μm at temperatures of 185, 215, and 245 K. The differences appear to be largest at 185 K, although the magnitudes of the differences are small compared to the benchmark values (Figure S1 in Supporting Information S1). Table S2 in Supporting Information S1 shows the root mean square error and mean bias error statistics for each scattering property, which are smaller than 0.002 and 0.000006, respectively. Based on the small interpolation errors in Table S2 in Supporting Information S1, relatively coarse spectral and temperature resolutions with the aforementioned 215 wavelengths and 12 temperatures can be used in developing an effective ice particle single-scattering property database suitable for use with the upcoming far-IR instruments.

The second sensitivity study described in Section 2 compares the bulk optical properties computed using the IY11 and the new ice refractive index compilation at 3 wavelengths, where the largest differences in the real or imaginary refractive index components are found, to illustrate possible effects of the new refractive index

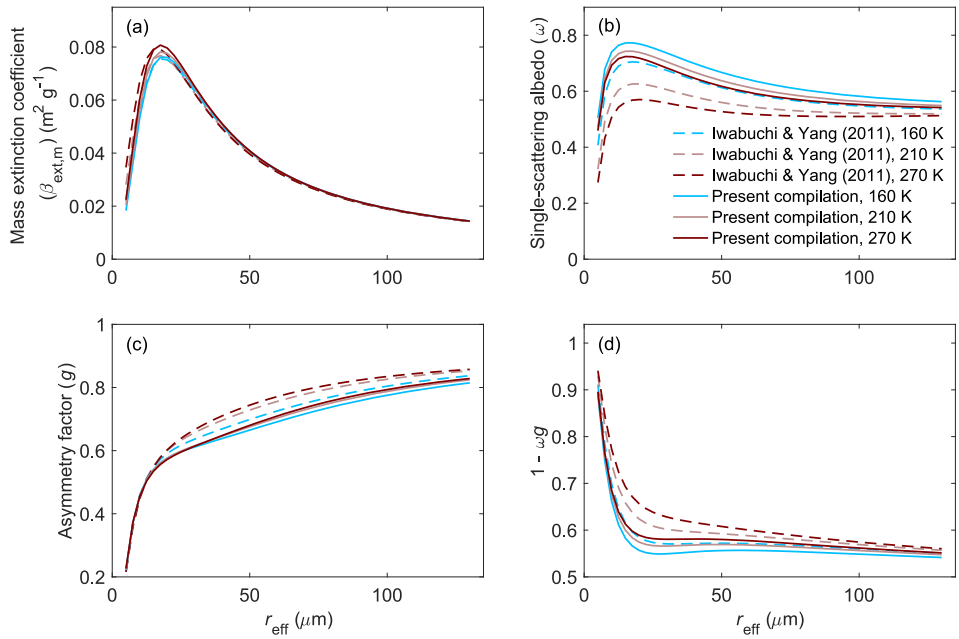

Figure 2. Variations of (a) $\beta_{ext,m}$ (m^2 g^{-1}), (b) ω, (c) g, and (d) 1–ωg with respect to r_{eff} (μm) at $\lambda = 90.1274$ μm. In each panel, solid and dashed curves are results computed using ice refractive index data from the present compilation and IY11; blue, brown, and maroon curves are results computed with the refractive index data at temperatures 160, 210, and 270 K, respectively.

compilation on a far-IR ice cloud optical model. To quantify the differences, we first perform IGOM and IITM computations for roughened hexagonal ice particles using ice refractive index data at 3 temperatures (160, 210, and 270 K) from IY11 and the new compilation in this study. The computations are performed at wavelength 70.4107 μm, around which n values in IY11 and the present compilation differ most in Figure 1a, and at wavelengths 45.3082 and 90.1274 μm, around which k values in these compilations differ most in Figure 1b. For given r_{eff} values of interest, associated Λ values satisfying Equations 1 and 2 can be found. With the Λ values, N (D_{max}) in Equation 1 can be used to calculate $\beta_{ext,m}$, ω, and g as in previous studies (e.g., Baum et al., 2005; Ren et al., 2023). In this study, we calculate $\beta_{ext,m}$, ω, and g for 51 r_{eff} values from 5 to 130 μm with an increment of 2.5 μm. Table S3 in Supporting Information S1 documents the Λ values associated with 26 of the 51 r_{eff} values. Note that if an ice particle shape other than the hexagonal column with an aspect ratio of 1 is chosen, $V(D_{max})$ and $A(D_{max})$ will be different and hence Λ values associated with r_{eff} values of interest need to be recalculated. In the Thompson microphysics scheme, Λ is determined by the prognostic cloud ice mass mixing ratio and number concentration. Thus, as Λ is determined in the microphysics scheme, the associated r_{eff} may be fed into the radiation scheme for the subsequent radiation computation, making the radiation computation more realistically reflect the ice cloud situation simulated by the model.

Figure 2 shows computed $\beta_{ext,m}$, ω, g, and (1–ωg) at $\lambda = 90.1274$ μm. Equivalent results at the other two wavelengths are provided in the supporting information (Figures S2 and S3 in Supporting Information S1). In the LW, ice cloud absorption and backscattering of surface-emitted radiation reduce the OLR and enhance the downwelling radiation at the surface. The smaller ω is, the more absorbing the ice cloud is and, hence the stronger this warming cloud radiative effect (CRE) is. Similarly, the smaller g is, the more backscattering the ice cloud is, and therefore, the stronger LW CRE is. In addition, given the same optical thickness, scattering media show similar apparent reflectance if the quantity (1–ωg) is conserved (van de Hulst, 1974). Therefore, the quantity (1–ωg) provides a proxy for the LW CRE at this wavelength (Tang et al., 2018). As shown in Figure 2a, Figures S2a and S3a in Supporting Information S1 the difference between $\beta_{ext,m}$ computed with our compilation and IY11 is smaller than 0.02 m^2 g^{-1} at all 3 selected wavelengths. Among the 3 selected wavelengths, the differences in ω, g, and (1–ωg) are largest at 90.1274 μm and the difference magnitude increases with increasing temperature. At $\lambda = 90.1274$ μm, ω computed with our compilation is higher than that computed with IY11 (Figure 2b), implying that the fractional ice cloud absorption in the present compilation is smaller. This result is consistent with the smaller k value in our

compilation than in IY11 at this wavelength (Figure 1b). At $\lambda = 45.3082$ μm, both n and k in our compilation are greater than in IY11 (Figure 1). Because ω is determined by both n and k, the associated value of ω is slightly higher than in IY11 at this wavelength (Figure S2b in Supporting Information S1). At all 3 wavelengths, g computed with our compilation is lower than in IY11 (Figure 2c, Figures S2c and S3c in Supporting Information S1). At $\lambda = 90.1274$ μm, the present compilation results in a weaker computed cloud radiative effect than in IY11 (Figure 2d). The ice refractive index compilation selection does not have a significant impact on the computed CRE at the other two wavelengths due to the compensation of the differences in ω and g (Figures S2d and S3d in Supporting Information S1). The computed CRE decreases with decreasing temperature at all 3 wavelengths (Figure 2d, Figures S2d and S3d in Supporting Information S1).

Figures S4–S6 in Supporting Information S1 show the differences in ice cloud bulk optical properties between the solid bullet rosette and hexagonal column shapes at the 3 wavelengths 45.3082, 70.4107, and 90.1274 μm, which are computed with the present ice refractive index compilation. Given the same cloud optical thickness and r_{eff}, an ice cloud consisting of bullet rosette particles has a smaller (1–ωg) and hence weaker LW CRE than an ice cloud consisting of hexagonal column particles at all 3 wavelengths (Figures S4–S6 in Supporting Information S1). Figures S7–S9 in Supporting Information S1 show the differences in hexagonal column ice cloud bulk optical properties computed with the particle size distributions from the MC6 cloud retrieval algorithm and the Thompson microphysics scheme at the 3 wavelengths, respectively. Given the same cloud optical thickness and r_{eff}, an ice cloud with the MC6 particle size distribution has a larger (1–ωg) and hence stronger LW CRE than an ice cloud with the Thompson scheme particle size distribution at all the 3 wavelengths (Figures S7–S9 in Supporting Information S1). Figures S10–S12 in Supporting Information S1 are same as Figures S7–S9 in Supporting Information S1 except for bullet rosette ice cloud bulk optical properties. A bullet rosette ice cloud with the MC6 particle size distribution also has a larger (1–ωg) and hence stronger LW CRE than one with the Thompson scheme particle size distribution except for $\lambda = 90.1274$ μm when $r_{\text{eff}} > 60$ μm (Figures S10–S12 in Supporting Information S1). Our results imply that particle size distribution has a more significant impact on the ice cloud bulk optical properties than ice particle shape and temperature (Figure 2 and Figures S2–S12 in Supporting Information S1).

4. Summary

This study compiles a new data set of temperature-dependent ice refractive indices across the solar and terrestrial wavelength range between 0.0443 and 2×10^6 μm. The development of the new data set is to facilitate forward ice crystal light-scattering computations for downstream applications to upcoming far-IR satellite missions, including efforts toward a more accurate modeling of the spectral variations of ice cloud optical properties and a better understanding of Earth's OLR under ice cloud conditions in polar regions.

We show the difference between a previous temperature-dependent refractive index compilation (i.e., IY11) and the present counterpart in the far-IR region, and the impacts of the far-IR ice refractive index differences on the computed bulk ice cloud optical properties. It appears that the differences between IY11 and the new refractive index compilation increase with increasing temperature and that consequently differences in the computed bulk ice cloud optical properties also increase with increasing temperature. However, the difference in computed longwave CRE is reduced due to a compensation of the differences in ω and g. Our results also imply that the temperature dependence of ice cloud bulk optical properties is a smaller, but still significant effect compared to accurate knowledge of particle size distribution. Assuming that the behavior of more realistic particle habits matches that seen for spherical particles, our work also implies that the computational demand associated with developing ice cloud optical properties from the new refractive indices can be reduced, as a selection of 12 temperatures (spanning the relevant atmospheric range) and 215 wavelengths in the far-IR region provides sufficient coverage to ensure accuracy in interpolated values of n and k.

Data Availability Statement

The new temperature-dependent ice refractive index compilation, sphere ice far-IR single-scattering property database, and hexagonal column ice single-scattering properties at 3 selected wavelengths are available at the Texas Data Repository (Wang et al., 2024).

Acknowledgments
This work is supported by the NASA Grant 80NSSC23K0651. We thank Hironobu Iwabuchi for his instruction on using the Kramers-Kronig relation analysis code he developed. Siheng Wang and Tong Ren thank Jiachen Ding, Yuheng Zhang, and James Coy for their instructions on using the light-scattering computational codes. We thank Steven Schroeder for helping edit this manuscript. We thank Charlie Zender and another anonymous reviewer for their constructive comments. The present light-scattering computations were performed with the Texas A&M High Performance Research Computing facilities. Helen Brindley is funded as part of Natural Environment Research Council's support for the National Centre for Earth Observation under Grant NE/R016518/1.

References

Abdelmonem, A., Järvinen, E., Duft, D., Hirst, E., Vogt, S., Leisner, T., & Schnaiter, M. (2016). PHIPS–HALO: The airborne particle habit imaging and polar scattering probe–Part 1: Design and operation. *Atmospheric Measurement Techniques*, *9*(7), 3131–3144. https://doi.org/10.5194/amt-9-3131-2016

Bantges, R. J., Brindley, H. E., Murray, J. E., Last, A. E., Russell, J. E., Fox, C., et al. (2020). A test of the ability of current bulk optical models to represent the radiative properties of cirrus cloud across the mid-and far-infrared. *Atmospheric Chemistry and Physics*, *20*(21), 12889–12903. https://doi.org/10.5194/acp-20-12889-2020

Baran, A. J. (2012). From the single-scattering properties of ice crystals to climate prediction: A way forward. *Atmospheric Research*, *112*, 45–69. https://doi.org/10.1016/j.atmosres.2012.04.010

Baran, A. J., Hill, P., Furtado, K., Field, P., & Manners, J. (2014). A coupled cloud physics–radiation parameterization of the bulk optical properties of cirrus and its impact on the met office unified model global atmosphere 5.0 configuration. *Journal of Climate*, *27*(20), 7725–7752. https://doi.org/10.1175/JCLI-D-13-00700.1

Baum, B. A., Yang, P., Heymsfield, A. J., Platnick, S., King, M. D., Hu, Y., & Bedka, S. T. (2005). Bulk scattering properties for the remote sensing of ice clouds. Part II: Narrowband models. *Journal of Applied Meteorology*, *44*(12), 1896–1911. https://doi.org/10.1175/JAM2309.1

Bi, L., & Yang, P. (2014). Accurate simulation of the optical properties of atmospheric ice crystals with the invariant imbedding T-matrix method. *Journal of Quantitative Spectroscopy and Radiative Transfer*, *138*, 17–35. https://doi.org/10.1016/j.jqsrt.2014.01.013

Bohren, C. F., & Huffman, D. R. (2008). *Absorption and scattering of light by small particles*. John Wiley and Sons.

Chen, X., Huang, X., & Flanner, M. G. (2014). Sensitivity of modeled far-IR radiation budgets in polar continents to treatments of snow surface and ice cloud radiative properties. *Geophysical Research Letters*, *41*(18), 6530–6537. https://doi.org/10.1002/2014GL061216

Cox, C., Harries, J., Taylor, J., Green, P., Baran, A., Pickering, J., et al. (2010). Measurement and simulation of mid-and far-infrared spectra in the presence of cirrus. *Quarterly Journal of the Royal Meteorological Society*, *136*(648), 718–739. https://doi.org/10.1002/qj.596

Coy, J., Saito, M., Yang, P., Liu, X., & Hu, Y. (2023). A robust ice cloud optical property model for Lidar-based remote sensing applications. *IEEE Geoscience and Remote Sensing Letters*, *21*, 1–5. https://doi.org/10.1109/LGRS.2023.3341506

Curtis, D. B., Rajaram, B., Toon, O. B., & Tolbert, M. A. (2005). Measurement of the temperature-dependent optical constants of water ice in the 15–200 μm range. *Appiled Optics*, *44*(19), 4102–4118. https://doi.org/10.1364/AO.44.004102

Dang, C., Fu, Q., & Warren, S. G. (2016). Effect of snow grain shape on snow albedo. *Journal of the Atmospheric Sciences*, *73*(9), 3573–3583. https://doi.org/10.1175/JAS-D-15-0276.1

Ding, J., Bi, L., Yang, P., Kattawar, G. W., Weng, F., Liu, Q., & Greenwald, T. (2017). Single-scattering properties of ice particles in the microwave regime: Temperature effect on the ice refractive index with implications in remote sensing. *Journal of Quantitative Spectroscopy and Radiative Transfer*, *190*, 26–37. https://doi.org/10.1016/j.jqsrt.2016.11.026

Fan, C., Chen, Y. H., Chen, X., Lin, W., Yang, P., & Huang, X. (2023). A refined understanding of the ice cloud longwave scattering effects in climate model. *Journal of Advances in Modeling Earth Systems*, *15*(10), e2023MS003810. https://doi.org/10.1029/2023MS003810

Foot, J. (1988). Some observations of the optical properties of clouds. II: Cirrus. *Quarterly Journal of the Royal Meteorological Society*, *114*(479), 145–164. https://doi.org/10.1002/qj.49711447908

Fu, Q. (1996). An accurate parameterization of the solar radiative properties of cirrus clouds for climate models. *Journal of Climate*, *9*(9), 2058–2082. https://doi.org/10.1175/1520-0442(1996)009<2058:AAPOTS>2.0.CO;2

Fu, Q., Yang, P., & Sun, W. (1998). An accurate parameterization of the infrared radiative properties of cirrus clouds for climate models. *Journal of Climate*, *11*(9), 2223–2237. https://doi.org/10.1175/1520-0442(1998)011<2223:AAPOTI>2.0.CO;2

Harries, J., Carli, B., Rizzi, R., Serio, C., Mlynczak, M., Palchetti, L., et al. (2008). The far-infrared Earth. *Reviews of Geophysics*, *46*(4). RG4004. https://doi.org/10.1029/2007RG000233

Huang, X., Loeb, N. G., & Yang, W. (2010). Spectrally resolved fluxes derived from collocated AIRS and CERES measurements and their application in model evaluation: 2. Cloudy sky and band-by-band cloud radiative forcing over the tropical oceans. *Journal of Geophysical ResearchAtmospheres*, *115*(D21), D21101. https://doi.org/10.1029/2010JD013932

Huang, X., Yang, W., Loeb, N. G., & Ramaswamy, V. (2008). Spectrally resolved fluxes derived from collocated AIRS and CERES measurements and their application in model evaluation: Clear sky over the tropical oceans. *Journal of Geophysical Research: Atmospheres*, *113*(D9), D09110. https://doi.org/10.1029/2007JD009219

Iwabuchi, H., & Yang, P. (2011). Temperature dependence of ice optical constants: Implications for simulating the single-scattering properties of cold ice clouds. *Journal of Quantitative Spectroscopy and Radiative Transfer*, *112*(15), 2520–2525. https://doi.org/10.1016/j.jqsrt.2011.06.017

Jackson, J. D. (1999). *Classical electrodynamics* (3rd ed.). John Wiely and Sons, Inc.

Järvinen, E., Jourdan, O., Neubauer, D., Yao, B., Liu, C., Andreae, M. O., et al. (2018b). Additional global climate cooling by clouds due to ice crystal complexity. *Atmospheric Chemistry and Physics*, *18*(21), 15767–15781. https://doi.org/10.5194/acp-18-15767-2018

Järvinen, E., Wernli, H., & Schnaiter, M. (2018). Investigations of mesoscopic complexity of small ice crystals in midlatitude cirrus. *Geophysical Research Letters*, *45*(20), 11–465. https://doi.org/10.1029/2018GL079079

Jiang, J. H., & Wu, D. L. (2004). Ice and water permittivities for millimeter and sub-millimeter remote sensing applications. *Atmospheric Science Letters*, *5*(7), 146–151. https://doi.org/10.1002/asl.77

Khuller, A. R., Christensen, P. R., & Warren, S. G. (2021). Spectral albedo of dusty Martian H_2O snow and ice. *Journal of Geophysical Research: Planets*, *126*(9), e2021JE006910. https://doi.org/10.1029/2021JE006910

Kuo, C. P., Yang, P., Huang, X., Feldman, D., Flanner, M., Kuo, C., & Mlawer, E. J. (2017). Impact of multiple scattering on longwave radiative transfer involving clouds. *Journal of Advances in Modeling Earth Systems*, *9*(8), 3082–3098. https://doi.org/10.1002/2017MS001117

Lawson, R., Woods, S., Jensen, E., Erfani, E., Gurganus, C., Gallagher, M., et al. (2019). A review of ice particle shapes in cirrus formed in situ and in anvils. *Journal of Geophysical Research: Atmospheres*, *124*(17–18), 10049–10090. https://doi.org/10.1029/2018JD030122

L'Ecuyer, T. S., Drouin, B. J., Anheuser, J., Grames, M., Henderson, D. S., Huang, X., et al. (2021). The polar radiant energy in the far infrared experiment: A new perspective on polar longwave energy exchanges. *Bulletin of the American Meteorological Society*, *102*(7), E1431–E1449. https://doi.org/10.1175/BAMS-D-20-0155.1

Loeb, N. G., Yang, P., Rose, F. G., Hong, G., Sun-Mack, S., Minnis, P., et al. (2018). Impact of ice cloud microphysics on satellite cloud retrievals and broadband flux radiative transfer model calculations. *Journal of Climate*, *31*(5), 1851–1864. https://doi.org/10.1175/JCLI-D-17-0426.1

Mätzler, C. (2006). *Thermal microwave radiation: Applications for remote sensing* (Vol. 52). The Institution of Engineering and Technology.

Palchetti, L., Brindley, H., Bantges, R., Buehler, S., Camy-Peyret, C., Carli, B., et al. (2020). FORUM: Unique far-infrared satellite observations to better understand how Earth radiates energy to space. *Bulletin of the American Meteorological Society*, *101*(12), E2030–E2046. https://doi.org/10.1175/BAMS-D-19-0322.1

Platnick, S., Meyer, K. G., King, M. D., Wind, G., Amarasinghe, N., Marchant, B., et al. (2017). The MODIS cloud optical and microphysical products: Collection 6 updates and examples from Terra and Aqua. *IEEE Transactions on Geoscience and Remote Sensing*, *55*(1), 502–525. https://doi.org/10.1109/TGRS.2016.2610522

Reinert, C., Mutschke, H., Krivov, A., Löhne, T., & Mohr, P. (2015). Absorption of crystalline water ice in the far infrared at different temperatures. *Astronomy and Astrophysics*, *573*, A29. https://doi.org/10.1051/0004-6361/201424276

Ren, T., Li, D., Muller, J., & Yang, P. (2021). Sensitivity of radiative flux simulations to ice cloud parameterization over the equatorial Western Pacific Ocean region. *Journal of the Atmospheric Sciences*, *78*(8), 2549–2571. https://doi.org/10.1175/JAS-D-21-0017.1

Ren, T., Yang, P., Garrett, K., Ma, Y., Ding, J., & Coy, J. (2023). A microphysics-scheme-consistent snow optical parameterization for the community radiative transfer model. *Monthly Weather Review*, *151*(2), 383–402. https://doi.org/10.1175/MWR-D-22-0145.1

Ren, T., Yang, P., Schumacher, C., Huang, X., & Lin, W. (2020). Impact of cloud longwave scattering on radiative fluxes associated with the Madden-Julian Oscillation in the Indian Ocean and maritime continent. *Journal of Geophysical Research: Atmospheres*, *125*(13), e2020JD032591. https://doi.org/10.1029/2020JD032591

Roemer, F. E., Buehler, S. A., Brath, M., Kluft, L., & John, V. O. (2023). Direct observation of Earth's spectral long-wave feedback parameter. *Nature Geoscience*, *16*(5), 416–421. https://doi.org/10.1038/s41561-023-01175-6

Saito, M., & Yang, P. (2022). Generalization of atmospheric nonspherical particle size: Interconversions of size distributions and optical equivalence. *Journal of the Atmospheric Sciences*, *79*(12), 3333–3349. https://doi.org/10.1175/JAS-D-22-0086.1

Saito, M., Yang, P., Huang, X., Brindley, H. E., Mlynczak, M. G., & Kahn, B. H. (2020). Spaceborne middle- and far-Infrared observations improving nighttime ice cloud property retrievals. *Geophysical Research Letters*, *47*(18), e2020GL087491. https://doi.org/10.1029/2020GL087491

Schnaiter, M., Järvinen, E., Abdelmonem, A., & Leisner, T. (2018). PHIPS-HALO: The airborne particle habit imaging and polar scattering probe–Part 2: Characterization and first results. *Atmospheric Measurement Techniques*, *11*(1), 341–357. https://doi.org/10.5194/amt-11-341-2018

Tang, G., Yang, P., Kattawar, G. W., Huang, X., Mlawer, E. J., Baum, B. A., & King, M. D. (2018). Improvement of the simulation of cloud longwave scattering in broadband radiative transfer models. *Journal of the Atmospheric Sciences*, *75*(7), 2217–2233. https://doi.org/10.1175/JAS-D-18-0014.1

Thompson, G., Field, P. R., Rasmussen, R. M., & Hall, W. D. (2008). Explicit forecasts of winter precipitation using an improved bulk microphysics scheme. Part II: Implementation of a new snow parameterization. *Monthly Weather Review*, *136*(12), 5095–5115. https://doi.org/10.1175/2008MWR2387.1

Thompson, G., Rasmussen, R. M., & Manning, K. (2004). Explicit forecasts of winter precipitation using an improved bulk microphysics scheme. Part I: Description and sensitivity analysis. *Monthly Weather Review*, *132*(2), 519–542. https://doi.org/10.1175/1520-0493(2004)132<0519:EFOWPU>2.0.CO;2

Thompson, G., Tewari, M., Ikeda, K., Tessendorf, S., Weeks, C., Otkin, J., & Kong, F. (2016). Explicitly-coupled cloud physics and radiation parameterizations and subsequent evaluation in WRF high-resolution convective forecasts. *Atmospheric Research*, *168*, 92–104. https://doi.org/10.1016/j.atmosres.2015.09.005

van de Hulst, H. C. (1974). The spherical albedo of a planet covered with a homogeneous cloud layer. *Astronomy and Astrophysics*, *35*, 209.

Wang, S., Ren, T., Yang, P., Saito, M., & Brindley, H. E. (2024). A new temperature-dependent ice refractive index compilation and associated ice particle single-scattering properties in the far-infrared. (Version 4) [Dataset]. *Texas Data Repository*. https://doi.org/10.18738/T8/QTPCNG

Warren, S. G. (1984). Optical constants of ice from the ultraviolet to the microwave. *Applied Optics*, *23*(8), 1206–1225. https://doi.org/10.1364/AO.23.001206

Warren, S. G. (2019). Optical properties of ice and snow. *Philosophical Transactions of the Royal Society A*, *377*(2146), 20180161. https://doi.org/10.1098/rsta.2018.0161

Warren, S. G., & Brandt, R. E. (2008). Optical constants of ice from the ultraviolet to the microwave: A revised compilation. *Journal of Geophysical Research: Atmospheres*, *113*(D14). https://doi.org/10.1029/2007JD009744

Wei, J., Ren, T., Yang, P., DiMarco, S. F., & Huang, X. (2023). Sensitivity of Arctic surface temperature to including a comprehensive ocean interior reflectance to the ocean surface albedo within the fully coupled CESM2. *Journal of Advances in Modeling Earth Systems*, *15*(12), e2023MS003702. https://doi.org/10.1029/2023MS003702

Wyser, K., & Yang, P. (1998). Average ice crystal size and bulk short-wave single-scattering properties of cirrus clouds. *Atmospheric Research*, *49*(4), 315–335. https://doi.org/10.1016/S0169-8095(98)00083-0

Yang, P., Bi, L., Baum, B. A., Liou, K.-N., Kattawar, G. W., Mishchenko, M. I., & Cole, B. (2013). Spectrally consistent scattering, absorption, and polarization properties of atmospheric ice crystals at wavelengths from 0.2 to 100 μm. *Journal of the Atmospheric Sciences*, *70*(1), 330–347. https://doi.org/10.1175/JAS-D-12-039.1

Yang, P., Ding, J., Panetta, R. L., Liou, K.-N., Kattawar, G. W., & Mishchenko, M. I. (2019). On the convergence of numerical computations for both exact and approximate solutions for electromagnetic scattering by nonspherical dielectric particles. *Progress in Electromagnetics Research*, *164*, 27–61. https://doi.org/10.2528/PIER18112810

Yang, P., & Liou, K. (1996). Geometric-optics–integral-equation method for light scattering by nonspherical ice crystals. *Applied Optics*, *35*(33), 6568–6584. https://doi.org/10.1364/AO.35.006568

Yang, P., Mlynczak, M. G., Wei, H., Kratz, D. P., Baum, B. A., Hu, Y. X., et al. (2003). Spectral signature of ice clouds in the far-infrared region: Single-scattering calculations and radiative sensitivity study. *Journal of Geophysical Research: Atmospheres*, *108*(D18). https://doi.org/10.1029/2002JD003291

Zender, C. S., & Kiehl, J. (1997). Sensitivity of climate simulations to radiative effects of tropical anvil structure. *Journal of Geophysical Research: Atmospheres*, *102*(D20), 23793–23803. https://doi.org/10.1029/97JD02009

Zhang, Y., Ding, J., Yang, P., & Panetta, R. L. (2022). Vector spherical wave function truncation in the invariant imbedding T-matrix method. *Optics Express*, *30*(17), 30020–30037. https://doi.org/10.1364/OE.459648

References From the Supporting Information

Clapp, M., Worsnop, D., & Miller, R. (1995). Frequency-dependent optical constants of water ice obtained directly from aerosol extinction spectra. *Journal of Physical Chemistry*, *99*(17), 6317–6326. https://doi.org/10.1021/j100017a010

Gosse, S., Labrie, D., & Chylek, P. (1995). Refractive index of ice in the 1.4–7.8-μm spectral range. *Applied Optics*, *34*(28), 6582–6586. https://doi.org/10.1364/AO.34.006582

Rajaram, B., Glandorf, D. L., Curtis, D. B., Tolbert, M. A., Toon, O. B., & Ockman, N. (2001). Absorption of crystalline water ice in the far infrared at different temperatures: New results and critical review of the available measurements. *Applied Optics*, *40*(25), 4449–4462. https://doi.org/10.1364/AO.40.004449

Toon, O. B., Tolbert, M. A., Koehler, B. G., Middlebrook, A. M., & Jordan, J. (1994). Infrared optical constants of H2O ice, amorphous nitric acid solutions, and nitric acid hydrates. *Journal of Geophysical Research: Atmospheres*, *99*(D12), 25631–25654. https://doi.org/10.1029/94JD02388